Demonstration of a frequency spectral compression effect through an up-conversion interferometer

Jean-Thomas Gomes,[1,*] Ludovic Grossard,[1] Damien Ceus,[1] Sébastien Vergnole,[1,2] Laurent Delage,[1] François Reynaud,[1] Harald Herrmann,[3] and Wolfgang Sohler[3]

[1]Xlim, Département Photonique, Université de Limoges, UMR CNRS 7252, 123 Av. Albert Thomas, 87060 Limoges CEDEX, France
[2]Current address: Horiba Scientific, 231 rue de Lille, 59650 Villeneuve d'Ascq, France
[3]Universität Paderborn, Angewandte Physik, Warburger Str. 100-33098 PADERBORN, Germany
[*]jean-thomas.gomes@unilim.fr

Abstract: This paper reports on the experimental implementation of an interferometer featuring sum frequency generation (SFG) processes powered by a pump spectral doublet. The aim of this configuration is to allow the use of the SFG process over an enlarged spectral domain. By analyzing the converted signal, we experimentally demonstrate a frequency spectral compression effect from the infrared input signal to the visible one converted through the SFG process. Recently, such a compression effect has been numerically demonstrated by Wabnitz et al. We also verify experimentally that we fully retrieve the temporal coherence properties of the infrared input signal in the visible field. The experimental setup permits to demonstrate an experimental frequency spectral compression factor greater than 4. This study takes place in the general field of coherence analysis through second order non-linear processes.

OCIS codes: (120.3180) Interferometry; (110.2650) Fringe analysis; (190.4223) Nonlinear wave mixing; (190.7220) Upconversion; (160.3730) Lithium niobate; (060.2310) Fiber optics.

References and links

1. M. A. Albota and F. N. C. Wong, "Efficient single-photon counting at 1.55 mm by means of frequency upconversion," Opt. Lett. **29,** 1449–1451 (2004).
2. A. P. VanDevender and P. G. Kwiat, "High efficiency single photon detection via frequency up-conversion," J. Mod. Opt. **51,** 1433–1452 (2004).
3. L. Ma, J. C. Bienfang, O. Slattery, and X. Tang, "Up-conversion single-photon detector using multi-wavelength sampling techniques," Opt. Express **19,** 5470–5479 (2011).
4. K.-D. Bchter, H. Herrmann, C. Langrock, M.M. Fejer, and W. Sohler, "All-optical Ti:PPLN wavelength conversion modules for free-space optical transmission links in the mid-infrared," Opt. Express **34,** 470–472 (2009).
5. S. Brustlein, L. Del Rio, A. Tonello, L. Delage, F. Reynaud, H. Herrmann, and W. Sohler, "Laboratory demonstration of an infrared-to-visible up-conversion interferometer for spatial coherence analysis," Phys. Rev. Lett. **100,** 153903 (2008).
6. D. Ceus, A. Tonello, L. Grossard, L. Delage, F. Reynaud, H. Herrmann, and W. Sohler, "Phase closure retrieval in an infrared-to-visible upconversion interferometer for high resolution astronomical imaging," Opt. Express **19,** 8616–8624 (2011).
7. R. T. Thew, H. Zbinden, and N. Gisin, "Tunable upconversion photon detector," Appl. Phys. Lett. **93,** 071104 (2008).

#181682 - $15.00 USD Received 19 Dec 2012; revised 17 Jan 2013; accepted 17 Jan 2013; published 31 Jan 2013

8. Q. Zhang, C. Langrock, M. M. Fejer, and Y. Yamamoto, "Waveguide-based single-pixel up-conversion infrared spectrometer," Opt. Express **16,** 19557–19561 (2008).
9. S. Wabnitz, A. Picozzi, A. Tonello, D. Modotto, and G. Millot, "Control of signal coherence in parametric frequency mixing with incoherent pumps: narrowband mid-infrared light generation by downconversion of broadband amplified spontaneous emission source at 1550 nm," J. Opt. Soc. Am. B **29,** 3128–3135, (2012).
10. R. W. Boyd, *Nonlinear Optics* (Academic Press, New York, 2008), pp. 69–96.
11. L. Del Rio, M. Ribiere, L. Delage, and F. Reynaud, "First demonstration of a temporal coherence analysis through a parametric interferometer," Opt. Commun. **281,** 2722–2726 (2008).
12. L. M. Simohamed, L. Delage, and F. Reynaud, "An optical delay line with a 318 mm stroke," Pure Appl. Opt. **5,** 1005–1009 (1996).
13. L. Delage, F. Reynaud, and A. Lannes, "A laboratory imaging stellar interferometer with fiber links," Appl. Opt. **39,** 6406–6420 (2000).
14. G. Huss, L. M. Simohamed, and F. Reynaud, "An all guided two-beam stellar interferometer: preliminary experiment," Opt. Commun. **182,** 71–82 (2000).
15. G. Huss, F. Reynaud, and L. Delage, "An all guided three-arm interferometer for stellar interferometry," Opt. Commun. **196,** 55–62 (2001).
16. M. Born and E. Wolf, *Principle of Optics* (Pergamon Press, London, 1964), pp. 503–504.

1. Introduction

Frequency conversion has been extensively used in the field of radio and microwave applications for a long time. This operation has been also achieved in the optical domain thanks to various nonlinear parametric interactions such as second harmonic, difference and sum frequency generation (SFG) in a nonlinear crystal or waveguide. In particular, SFG in a periodically poled Lithium Niobate (PPLN) crystal or waveguide allowed to convert an infrared wave into a visible one by using a pump source as shown in many applications [1–4].

In the field of high resolution imaging, we have recently demonstrated the ability to analyze the coherence properties of an infrared source through an up-conversion process in a two and a three-arm interferometer [5,6]. All over these first experiments, we were limited by the intrinsic spectral acceptance of the PPLN waveguides: if a large spectral bandwidth source at infrared wavelengths is converted through a SFG process with a single line pump, the PPLN spectral acceptance limits the nonlinear effect to a very narrow spectral bandwidth of the source. To overcome this spectral limitation, several techniques have already been proposed, involving an up-conversion detector which samples [7] or scans [8] the input signal spectrum by using a tunable pump laser.

As a long term goal we intend to study a SFG process powered by a pump frequency comb to increase the spectral bandwidth to be analyzed while preserving signal coherence information.

Wabnitz et al. have recently demonstrated numerically that the use of a non-monochromatic pump source to power a SFG process, converting a large spectral bandwidth infrared signal, leads to a frequency spectral compression of the converted wave through the non-linear process [9].

We intend here to experimentally demonstrate this frequency spectral compression behaviour through a SFG process. We use a pump spectral doublet to convert an input spectral doublet. In this configuration, each line of the pump spectral doublet addresses a single line of the input spectral doublet. Through the signal temporal coherence analysis, we experimentally demonstrate the frequency spectral compression effect and we verify that the temporal coherence information of the infrared signal is fully retrieved in the converted visible field.

2. Simulation results

The sum frequency generation is a non-linear process where a signal and a pump wave interact in a non-linear medium to generate a converted wave [10]. If ν_s and ν_p are the frequencies of the signal and pump waves respectively, the frequency of the converted wave is inferred from the

#181682 - $15.00 USD Received 19 Dec 2012; revised 17 Jan 2013; accepted 17 Jan 2013; published 31 Jan 2013

energy conservation law: $\nu_c = \nu_s + \nu_p$. The conversion efficiency strongly depends on the phase mismatch between the three interacting waves. In a PPLN waveguide, this phase mismatch is given by

$$\Delta k = \frac{2\pi}{c}\left(n_c\nu_c - n_s\nu_s - n_p\nu_p + \frac{c}{\Lambda}\right) \tag{1}$$

where n_c, n_s and n_p are the refractive indices of the fundamental modes in the Lithium Niobate waveguides at the converted, signal and pump frequencies respectively. Λ is the poling period of the PPLN. Thus, the normalized power conversion efficiency can be expressed as

$$\eta(\nu_s, \nu_p) = \mathrm{sinc}^2\left(\frac{\Delta kL}{2}\right) \tag{2}$$

where L is the PPLN length. For a given pump frequency, the full width at half maximum (FWHM) of the main lobe of the $\eta(\nu_s)$ curve defines the frequency spectral acceptance, i.e. the spectral signal bandwidth over which a significant conversion efficiency is observed. Figure 1 shows a color-map of the normalized conversion efficiency for any signal/pump couple around the mean pump frequency $\nu_p^0 = 281,76$ THz ($\lambda_p^0 = 1064.0$ nm) and the mean signal frequency $\nu_s^0 = 194.35$ THz ($\lambda_s^0 = 1542.5$ nm).

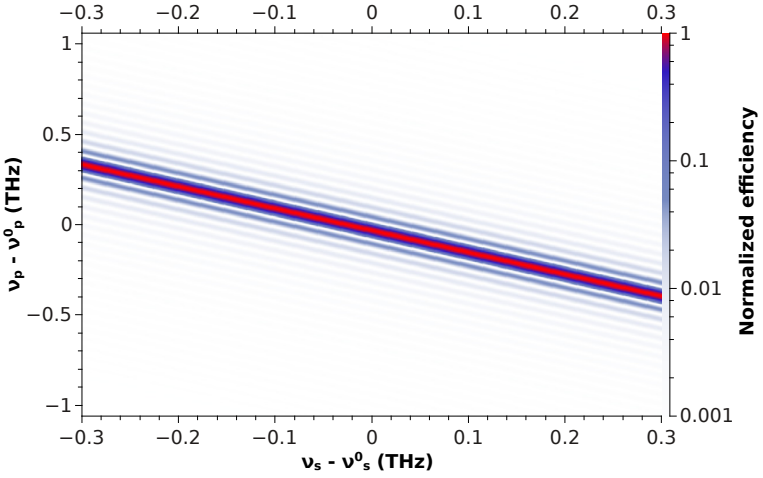

Fig. 1. Normalized simulated sum frequency generation efficiency. The signal frequency ν_s (horizontal axis) is centered on $\nu_s^0 = 194.35$ THz ($\lambda_s^0 = 1542.5$ nm), and the pump frequency ν_p (vertical axis) is centered on $\nu_p^0 = 281.76$ THz ($\lambda_p^0 = 1064.0$ nm). The converted frequency is not represented here. For a perfect phase matching (red curve), ν_p depends linearly on ν_s

It is worth noting that the converted frequency is not represented here, but can be inferred from the energy conservation law for each pump/signal frequency couple. Here, the converted light frequency is centered on $\nu_c = 476.11$ THz ($\lambda_c = 629.7$ nm). This simulation has been conducted for a 4 cm long PPLN waveguide. The poling period was $\Lambda = 10.85$ μm. In these conditions, the frequency spectral acceptance is equal to 38 GHz (wavelength spectral acceptance equal to 0.3 nm at $\lambda_s = 1542.5$ nm). This conversion efficiency map is directly related to the waveguide mode dispersion, mainly determined by the Lithium Niobate index dispersion and the PPLN poling period.

The red curve represents the maximum conversion efficiency, where the three interacting waves are perfectly phase matched ($\Delta k = 0$). In the pump and signal frequency ranges used here, this curve can be fitted by a linear function:

#181682 - $15.00 USD Received 19 Dec 2012; revised 17 Jan 2013; accepted 17 Jan 2013; published 31 Jan 2013

$$\nu_p = a + b_{num}\nu_s \tag{3}$$

Then, the energy conservation law writes

$$\nu_c = a + (1 + b_{num})\nu_s \tag{4}$$

Let us consider now an input signal with a large spectral width $\Delta\nu_s$. We assume that the pump spectrum is flat and sufficiently broad to convert each frequency of the input signal with a maximum conversion efficiency. The spectral width of the converted field is then given by

$$\Delta\nu_c = (1 + b_{num})\Delta\nu_s \tag{5}$$

The converted spectrum undergoes a spectral compression by a factor

$$\rho_{num} = \frac{\Delta\nu_s}{\Delta\nu_c} = |\frac{1}{1 + b_{num}}| \tag{6}$$

The numerically estimated spectral compression factor ρ_{num} depends on the slope b_{num} which is directly linked to the chromatic dispersion properties of the Lithium Niobate waveguide through Eq. (1). Here, a linear regression gives $b_{num} = -1.213$, leading to a compression factor $\rho_{num} = 4.70$. Note that here b_{num} is negative, which means that the converted spectrum is also frequency–flipped.

The use of a broad pump spectrum is mandatory to obtain the frequency spectral compression effect. Indeed, with a monochromatic pump, the slope b_{num} is not defined and there is no frequency compression, as it has been investigated in [9] and [11].

3. Experimental setup

To experimentally retrieve the theoretical frequency compression effect reported in the previous section, we implemented an experimental setup based on the up-conversion interferometer previously developed in our laboratory [5, 6, 11]. In the current setup, the pump is composed of a spectral doublet to convert one input signal composed of two different frequency lines.

This interferometric configuration has two main goals. The first one is to experimentally demonstrate the frequency spectral compression [9]. Indeed, the line frequency separation change between the input and converted doublets can be extracted from the analysis of the fringe pattern envelopes [11]. The second goal is to validate that such a compression effect through the SFG preserves the temporal coherence of the input infrared field.

The setup is based on a Mach-Zehnder interferometer as shown on Fig. 2. The infrared spectral doublet under study is composed of a set of two balanced distributed-feedback (DFB) lasers lines at $\lambda_{s1} = 1542.12$ nm ($\nu_{s1} = 194.40$ THz) and $\lambda_{s2} = 1543.81$ nm ($\nu_{s2} = 194.19$ THz). The pump spectral doublet is also composed of two balanced DFB lasers lines with an emission at $\lambda_{p1} = 1063.3$ nm ($\nu_{p1} = 281.95$ THz) and $\lambda_{p2} = 1064.3$ nm ($\nu_{p2} = 281.68$ THz).

The infrared input signal and the pump source are both equally shared between the two interferometric arms by two polarization maintaining and single-mode fiber couplers at their operating wavelength. A 10-cm stroke fibered delay line is inserted in the arm #2 to adjust the optical path difference (OPD) between the two arms in the infrared stage of the interferometer [12]. An optical path modulator (OPM) [13], with a 100-μm stroke, is inserted in the same arm for a fine OPD adjustment and to induce a temporal optical path modulation on the input signal. This allows to display the fringe pattern as a function of time. This device is driven by a triangular high voltage to induce sequenced linear OPDs as a function of time.

#181682 - $15.00 USD Received 19 Dec 2012; revised 17 Jan 2013; accepted 17 Jan 2013; published 31 Jan 2013

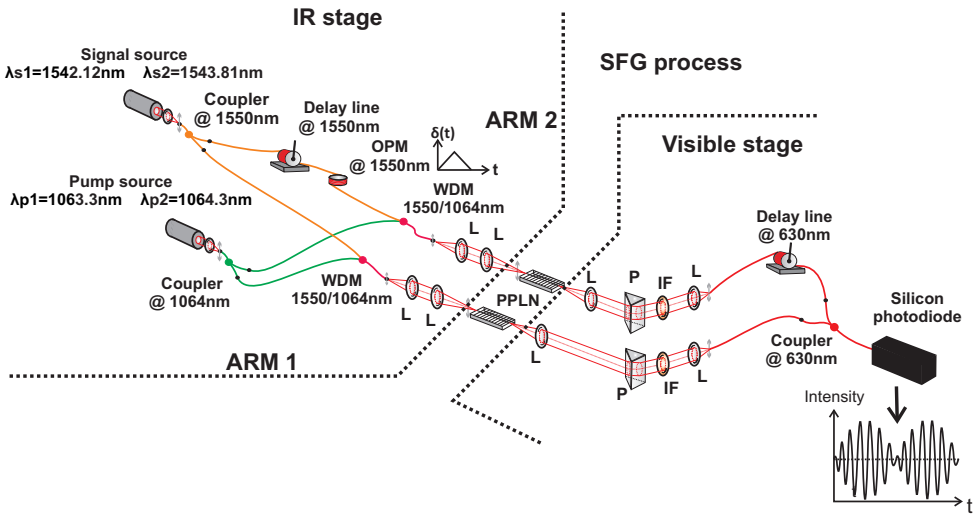

Fig. 2. Experimental setup of the up-conversion interferometer. OPM: optical path modulator, WDM: wavelength division multiplexer, L: lens, P: prism, IF: interference filter

The infrared signal and pump sources are spectrally multiplexed together thanks to polarization maintaining fibered wavelength division multiplexers (WDM) before SFG stages on each arm of the interferometer.

In each arm, the emerging multiplexed beams are focused by achromatic injection systems in a 4 cm long Ti-indiffused PPLN waveguide with a spectral acceptance of 0.3 nm (38 GHz) around 1542.5 nm. The two non linear crystals are placed in thermally regulated enclosures to ensure a proper phase matching and achieve exactly the same expected SFG process on each arm of the interferometer. In this configuration, each line of the pump spectral doublet addresses a single line of the infrared spectral doublet to convert. We plotted the two experimental signal/pump couples on the normalized PPLN conversion efficiency curve described in the previous section (Fig. 3).

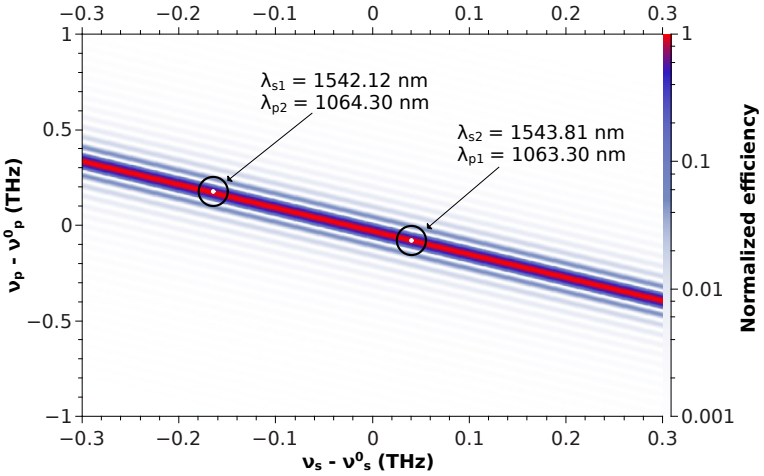

Fig. 3. Positions of the experimental pump/signal couples on the normalized conversion efficiency curve linked to the PPLN waveguides

#181682 - $15.00 USD Received 19 Dec 2012; revised 17 Jan 2013; accepted 17 Jan 2013; published 31 Jan 2013

The emerging up-converted signals around $\lambda_c = 629.7$ nm ($\nu_c = 476.11$ THz) are spectrally selected on each arm by a spectral filtering stage, composed of a dispersive prisms (P) and an interference filter (IF) centered on the mean converted wavelength. After this stage, the converted signals are spatially filtered thanks to single-mode polarization maintaining fibers at the converted wavelength. We have inserted another fiber delay line on arm #2, with a 10-cm stroke to control the OPD between the two arms of the interferometer on the visible stage. At the output of the up-conversion interferometer, we combine the two visible optical fields thanks to a polarization maintaining and single-mode fiber coupler. The resulting fringe pattern is then detected by a Silicon photodiode.

4. Demonstration of the frequency spectral compression effect

4.1. Phase propagation through the up-conversion interferometer

In this section, we explain how we can infer the frequency spectral compression effect thanks to the contrast evolution measurements as a function of the OPD applied before or after the SFG process. We focus our study on the phase propagation term of the two waves at frequencies ν_{s1} and ν_{s2}, assuming the same intensity I_0 through the two arms of the up-conversion interferometer. The equations below show the theoretical expressions of the phase terms as a function of the optical path on each stage and each arm (δ_{IR1}, δ_{IR2}, δ_{Vi1}, δ_{Vi2}) for the input and output spectral doublet (ν_{s1}, ν_{s2} and ν_{c1}, ν_{c2}).

	Infrared stage (ν_s)	Visible stage (ν_c)
arm 1	$\varphi_{1s1} = \frac{2\pi}{c} \cdot \nu_{s1} \cdot \delta_{IR1}$ $\varphi_{1s2} = \frac{2\pi}{c} \cdot \nu_{s2} \cdot \delta_{IR1}$	$\varphi_{1c1} = \frac{2\pi}{c} \cdot \nu_{c1} \cdot \delta_{Vi1}$ $\varphi_{1c2} = \frac{2\pi}{c} \cdot \nu_{c2} \cdot \delta_{Vi1}$
arm 2	$\varphi_{2s1} = \frac{2\pi}{c} \cdot \nu_{s1} \cdot \delta_{IR2}$ $\varphi_{2s2} = \frac{2\pi}{c} \cdot \nu_{s2} \cdot \delta_{IR2}$	$\varphi_{2c1} = \frac{2\pi}{c} \cdot \nu_{c1} \cdot \delta_{Vi2}$ $\varphi_{2c2} = \frac{2\pi}{c} \cdot \nu_{c2} \cdot \delta_{Vi2}$
Phase difference ($\Delta\varphi = \varphi_2 - \varphi_1$)	$\Delta\varphi_{s1} = \frac{2\pi}{c} \cdot \nu_{s1} \cdot (\delta_{IR2} - \delta_{IR1})$ $\Delta\varphi_{s2} = \frac{2\pi}{c} \cdot \nu_{s2} \cdot (\delta_{IR2} - \delta_{IR1})$	$\Delta\varphi_{c1} = \frac{2\pi}{c} \cdot \nu_{c1} \cdot (\delta_{Vi2} - \delta_{Vi1})$ $\Delta\varphi_{c2} = \frac{2\pi}{c} \cdot \nu_{c2} \cdot (\delta_{Vi2} - \delta_{Vi1})$

The OPM temporally modulates the phase of the input infrared signal on arm #2 and the optical path on this arm can be written as $\delta_{IR2} = \delta^0_{IR2} + \delta(t)$. Thanks to the property of phase conservation in a sum frequency generation process [11], the phase differences on the infrared stage ($\Delta\varphi_{s1}$, $\Delta\varphi_{s2}$) are transferred to the input of the visible stage on each arm of the interferometer. Then, the fringe pattern at the output of the interferometer can be written for each frequency ν_{s1} and ν_{s2} as a function of the optical path variation

$$I_1(\delta) = 2 \cdot I_0 \cdot (1 + \cos(\Delta\varphi_{s1} + \Delta\varphi_{c1})) \tag{7}$$

$$I_2(\delta) = 2 \cdot I_0 \cdot (1 + \cos(\Delta\varphi_{s2} + \Delta\varphi_{c2})) \tag{8}$$

The resulting interferometric signal *Itot* at the output of the interferometer is equal to the incoherent sum of these two fringe systems. The mathematical expression of the resulting signal

#181682 - $15.00 USD Received 19 Dec 2012; revised 17 Jan 2013; accepted 17 Jan 2013; published 31 Jan 2013

Itot contains an envelope term $\mathscr{E}(\delta)$ modulating the fringes $\mathscr{F}(\delta)$. In the following, we focus on the envelope term expression and write $Itot(\delta)$ as

$$Itot(\delta) = I_1(\delta) + I_2(\delta) = 4 \cdot I_0 \cdot (1 + \mathscr{E}(\delta) \cdot \mathscr{F}(\delta)) \tag{9}$$

$$\text{with} \quad \mathscr{E}(\delta) = \cos\left(\frac{\pi \cdot \Delta\delta_{IR}}{L_{bIR}} + \frac{\pi \cdot \Delta\delta_{Vi}}{L_{bVi}}\right) \tag{10}$$

$$\text{and} \quad \mathscr{F}(\delta) = \cos\left(\frac{2\pi}{c} \cdot \Delta\delta_{IR} \cdot \overline{\nu_s} + \frac{2\pi}{c} \cdot \Delta\delta_{Vi} \cdot \overline{\nu_c}\right) \tag{11}$$

where $\overline{\nu_s} = (\nu_{s1} + \nu_{s2})/2$, $\overline{\nu_c} = (\nu_{c1} + \nu_{c2})/2$, $\Delta\delta_{IR} = \delta_{IR2} - \delta_{IR1}$, $\Delta\delta_{Vi} = \delta_{Vi2} - \delta_{Vi1}$, $L_{bIR} = c/\Delta\nu_s$, $L_{bVi} = c/\Delta\nu_c$, $\Delta\nu_s = \nu_{s1} - \nu_{s2}$ and $\Delta\nu_c = \nu_{c1} - \nu_{c2}$.

The contrast evolution of the fringe pattern is driven by the two different beat lengths related to the signal wave before and after the SFG process. When applying an OPD between the two interferometric arms on the infrared stage, the envelope period is equal to the beat length L_{bIR}. Conversely, when applying an OPD on the visible stage, the envelope period is equal to the beat length L_{bVi}. Due to the phase matching condition in the experimental configuration, the frequency spectral separations $\Delta\nu_s$ and $\Delta\nu_c$ are different before and after, the SFG process, and therefore the beat lengths are different between the infrared and the converted signals. Consequently, an OPD applied before and after SFG will not have the same impact on the fringe visibility, demonstrating a frequency spectral compression effect.

4.2. Experimental results

In a first step, we measured the maximum fringe contrast at the up-conversion interferometer output for a single line infrared signal (ν_{s1}) converted thanks to a single line pump source (ν_{p2}). The aim of this measurement was to calibrate the reliability of the setup. In this configuration, we obtained a contrast equal to 98.2%. When operating simultaneously with the two frequency pairs (ν_{s1}-ν_{p2} and ν_{s2}-ν_{p1}), the maximum contrast reached 98%. The contrast loss can be explained by a polarization control defect over the visible stage of the interferometer [14, 15]. However, these results prove our ability to implement several SFG processes simultaneously in the up-conversion interferometer arms while preserving a high contrast level.

To demonstrate the frequency spectral compression effect, we conducted measurements of the fringe contrast evolution for a balanced infrared spectral doublet. We measured the fringe contrast evolution as a function of the OPD between the two arms of the interferometer by applying this OPD either on the infrared stage or on the visible stage.

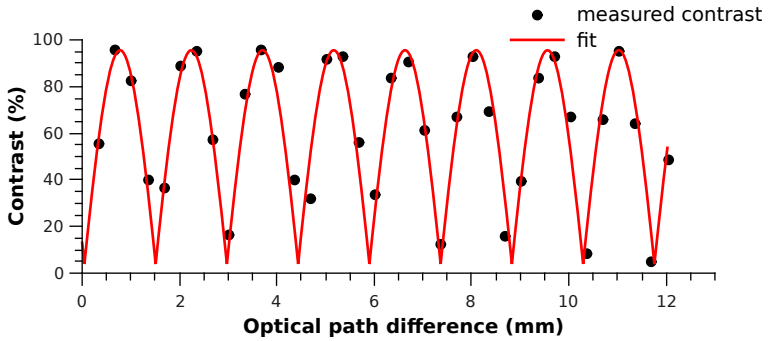

Fig. 4. Experimental fringe contrast versus the OPD applied on the infrared stage. Dots represent the measured contrasts. The red curve is the best theoretical fit. The beat length, which is equal to the contrast period, is $L_{bIR} = 1.46$ mm

#181682 - $15.00 USD Received 19 Dec 2012; revised 17 Jan 2013; accepted 17 Jan 2013; published 31 Jan 2013

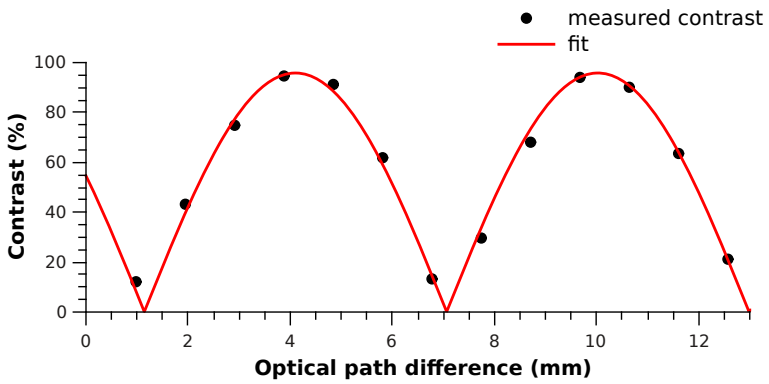

Fig. 5. Experimental fringe contrast versus the OPD applied on the visible stage. Dots represent the measured contrasts. The red curve is the best theoretical fit. The beat length, which is equal to the contrast period, is $L_{bVi} = 5.97$ mm

Figure 4 shows the experimental fringe contrast versus the OPD applied on the infrared stage. The beat length of the fringe pattern envelope is equal to $L_{bIR} = 1.46$ mm. When the OPD is applied on the visible stage (Fig. 5), the beat length L_{bVi} is equal to 5.97 mm. The periodicity difference between these contrast curves experimentally demonstrates a frequency spectral compression effect resulting from a multipump configuration in a sum frequency generation process. The experimental frequency spectral compression factor ρ_{exp} is equal to

$$\rho_{exp} = \frac{L_{bVi}}{L_{bIR}} = 4.09 \tag{12}$$

We note here a relative difference ($\approx 12.8\%$) with the simulated frequency compression factor $\rho_{num} = 4.70$. This difference is mainly due to the fact that each frequency couple ν_{s1}-ν_{p2} and ν_{s2}-ν_{p1} is not perfectly located on the maximum conversion efficiency curve (Fig. 3) because of the wavelength resolution limit (≈ 50 pm corresponding to ≈ 6.3 GHz at 1542.5 nm) on the DFB sources. The experimental slope b_{exp}, deduced from the signal/pump couple positions on Fig. 3, is equal to -1.245 instead of the previously numerically obtained slope $b_{num} = -1.213$ (relative difference of 2.6% between the two slopes). As the frequency spectral compression factor depends on this conversion efficiency slope, we retrieve the experimental conditions

$$\rho'_{exp} = \left|\frac{1}{1+b_{exp}}\right| = 4.08 \tag{13}$$

which is in very good agreement with the previous experimental frequency spectral compression factor deduced from the beat length measurement (relative difference between numerical and experimental results lower than 0.25%), attesting the correctness of the experimental results.

5. Demonstration of the temporal coherence information conservation

To experimentally verify that the converted field carries the same temporal coherence information than the input infrared field, we measured the contrast evolution as a function of an OPD applied on the infrared stage in one hand and on the visible stage in the other hand. To obtain a clearly identifiable temporal coherence signature, we strongly unbalanced the input signal doublet. The relation between the intensity of each line at ν_{s1} (I_1^0) and ν_{s2} (I_2^0) is now $I_1^0 = \alpha \cdot I_2^0$, with α the unbalance ratio between the two line intensities.

#181682 - $15.00 USD Received 19 Dec 2012; revised 17 Jan 2013; accepted 17 Jan 2013; published 31 Jan 2013

5.1. *Experimental results*

We unbalanced the infrared spectral doublet at the interferometer input by a factor $\alpha = 13.5$. In a first step, we measured the contrast evolution at the interferometer output as a function of an OPD applied on the infrared stage of the setup (Fig. 6). The constrast modulation amplitude is equal to 6.24%. The red curve represents the theoretical visibility function $V(\delta)$ of the fringe pattern contrast evolution calculated for the experimental conditions, using the Wiener-Khintchine theorem [16]

$$V(\delta) = |TF\,[PSD(\nu)]\,| \tag{14}$$

where $PSD(\nu)$ is the signal power spectral density, i.e. an unbalanced doublet by a factor $\alpha = 13.5$. This theoretical curve takes the interferometer defects into account and fits well with the measured contrast evolution.

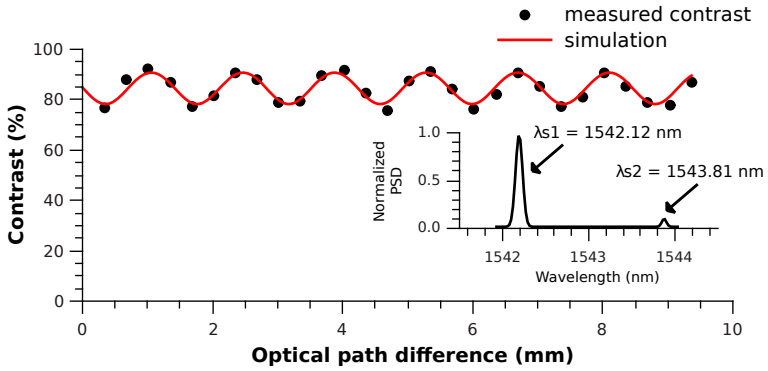

Fig. 6. Experimental fringe contrast versus the OPD applied on the infrared stage for an unbalance ratio $\alpha = 13.5$. Dots represent the measured contrast. The red curve is the theoretical contrast evolution obtained from the Wiener-Khintchine theorem for the same configuration than the experimental setup. The constrast modulation amplitude is equal to 6.24%. Inset shows the normalized power spectral density of the infrared spectral doublet under analyze.

In a second step, we conducted a measurement of the contrast evolution as a function of an OPD applied on the visible stage (Fig. 7).

The contrast modulation amplitude is equal to 6.09%, to be compared with the 6.24% modulation amplitude obtain when applying the OPD on the infrared stage. These results are in very good agreement (relative difference of 2.4%). We retrieve the same modulation amplitude before and after the SFG process, that clearly demonstrates the conservation of the temporal coherence information of the signal through a SFG process powered by a pump spectral doublet.

Finally, the beat length measured when the OPD is applied on the infrared stage (resp. on the visible stage) is $L_{bIR} = 1.43$ mm (resp. $L_{bVi} = 5.79$ mm), leading to a frequency spectral compression factor $\rho_{exp} = L_{bVi}/L_{bIR} = 4.05$. This result is in good agreement with the experimental value $\rho_{exp} = 4.09$ obtained in section 4 (relative difference between the two measurements lower than 1.5%) and demonstrates the reliability of the experimental setup.

#181682 - $15.00 USD Received 19 Dec 2012; revised 17 Jan 2013; accepted 17 Jan 2013; published 31 Jan 2013

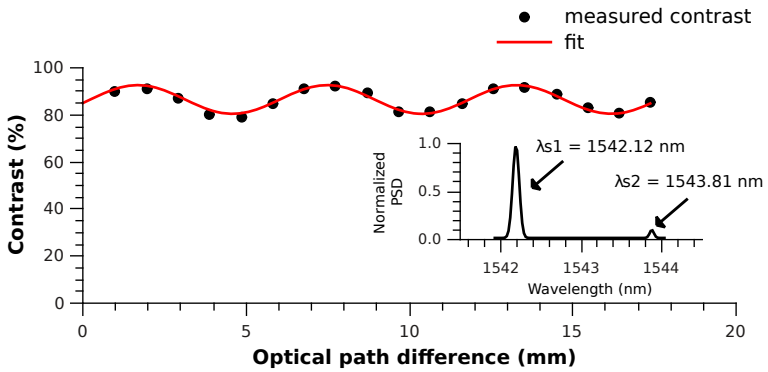

Fig. 7. Experimental fringe contrast versus the OPD applied on the infrared stage for an unbalance ratio $\alpha = 13.5$. Dots represent the measured contrasts. The red curve is the best theoretical fit. The constrast modulation amplitude is equal to 6.09%. Inset shows the normalized power spectral density of the infrared spectral doublet under analyze.

6. Conclusion

In this paper, we have numerically and experimentally demonstrated the frequency spectral compression effect of an infrared signal through a SFG process powered by a pump spectral doublet. We obtained an experimental compression factor $\rho_{exp} = 4.09$ with a high reliability.

We also verified that this compression effect does not deteriorate temporal coherence information of the infrared input signal under analyze and will permit to relax the constraints on the optical path equalization in a fibered interferometer, allowing an easier implementation while analyzing a broadband source.

Moreover, analyzing a broadband infrared source through an up-conversion interferometer, powered by a pump source in multipump configuration, will permit to benefit from a maximum frequency compression effect [9], increasing the coherence length of the source, while preserving its temporal coherence information.

Acknowledgments

This work has been financially supported by the Centre National d'Études Spatiales (CNES) and by the Institut National des Sciences de l'Univers (INSU). Our thanks go to A. Dexet for the development and his advices for all the specific mechanical components.

#181682 - $15.00 USD Received 19 Dec 2012; revised 17 Jan 2013; accepted 17 Jan 2013; published 31 Jan 2013